Journal of Hazardous Materials 460 (2023) 132308

Contents lists available at ScienceDirect

Journal of Hazardous Materials

journal homepage: www.elsevier.com/locate/jhazmat

Pyrolysis temperature and biochar redox activity on arsenic availability and speciation in a sediment

Matheus B. Soares [a,b,*], Owen W. Duckworth [b], Miroslav Stýblo [c], Peter H. Cable [c], Luís R.F. Alleoni [a]

[a] Department of Soil Science, Luiz de Queiroz College of Agriculture (ESALQ), University of São Paulo (USP), 13418900 Piracicaba, SP, Brazil
[b] Department of Crop and Soil Sciences, North Carolina State University, 27695 Raleigh, NC, USA
[c] Department of Nutrition, Gillings School of Global Public Health, University of North Carolina at Chapel Hill, 27599-7461 Chapel Hill, NC, USA

HIGHLIGHTS

- The application of biochar affects the reduction of As methylation.
- The redox fluctuation may favor the effectiveness of biochar.
- The pyrolysis temperature affects the spatial distribution of carbon contents.
- The application of biochar favors the reduction and dispersion of Fe(III) minerals.

GRAPHICAL ABSTRACT

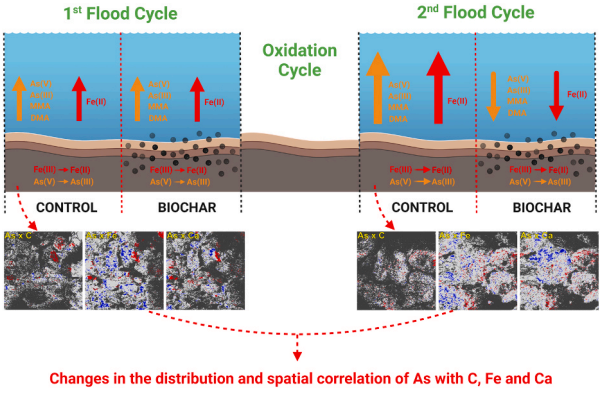

ARTICLE INFO

Editor: Anett Georgi

Keywords:
Arsenic methylation
Spatial variability
TOF-SIMS
DMA
MMA

ABSTRACT

Biochar is widely used for water and soil remediation in part because of its local availability and low production cost. However, its effectiveness depends on physicochemical properties related to its feedstock and pyrolysis temperature, as well as the environmental conditions of its use site. Furthermore, biochar is susceptible to natural aging caused by changes in soil or sediment moisture, which can alter its redox properties and interactions with contaminants such as arsenic (As). In this study, we investigated the effect of pyrolysis temperature and biochar application on the release and transformations of As in contaminated sediments subjected to redox fluctuations. Biochar application and pyrolysis temperature played an important role in As species availability, As methylation, and dissolved organic carbon concentration. Furthermore, successive flooding cycles that induced reductive conditions in sediments increased the As content in the solution by up to seven times. In the solid phase, the application of biochar and the flooding cycle altered the spatial distribution and speciation of carbon, iron (Fe) and As. In general, the application of biochar decreased the reduction of Fe(III) and As(V) after the first

* Correspondence to: University of São Paulo (USP), 13418900 Piracicaba, SP, Brazil.
E-mail address: bortolanza@usp.br (M.B. Soares).

https://doi.org/10.1016/j.jhazmat.2023.132308
Received 13 May 2023; Received in revised form 28 July 2023; Accepted 13 August 2023
Available online 18 August 2023

cycle of flooding. Our results demonstrate that the flooding cycle plays an important role in the reoxidation of biochar to the point of enhancing the immobilization of As.

1. Introduction

The contamination of soils, sediments, and water with potentially toxic elements (PTEs) is a serious global environmental, agricultural, and public health problem [1]. Arsenic (As), especially the inorganic species, is of particularly acute concern because of its cytotoxic, genotoxic, and mutagenic effects, resulting in negative health impacts such as increased risk of kidney, skin, lung, and bladder cancer [2]. Recent estimates show that more than 200 million people in at least 105 countries are exposed to As from contaminated water [3], highlighting the scope of the problem.

The redox-driven speciation of As in soil and sediment large dictates its mobility and bioavailability. In general, As is present in the soil as inorganic arsenate and arsenite [4], with the latter reduced species generally considered to be more mobile. The distribution of species and thus mobility of As is partially controlled by biogeochemical conditions of the environment, such as redox state (Eh) [5] The presence of organic C in the environment can, directly and indirectly, impact the As availability in the environment. Dissolved organic carbon (DOC) can directly promote the reduction of arsenate to arsenite as well as compete with As for binding sites on mineral surfaces [6]. Additionally, the addition of organic C in the environment can promote microbial metabolic processes responsible for As reduction and methylation [7], thus favoring the mobilization of inorganic As from the solid phase to the solution.

Redox cycling commonly results from the inundation and drying of soils and sediments. In Brazil, most As contamination is associated with mining tailings, often associated with gold extraction. Recent collapses of two tailings dams located in southeastern Brazil [8] have been associated with contamination of rivers close to the dams ([As] =10.4–50.4 $\mu g\ L^{-1}$ [9]). The rupture of these dams may also result in the deposition of contaminated sediments in other environments redox-sensitive environments, such as downstream estuaries [10]. It is thus necessary to better understand how As behaves in sediments undergoing redox fluctuations as well as develop redemption strategies that are robust under differing Eh conditions.

Biochar is an ecologically friendly soil and sediment amendment used in remediation by promoting surface complexation, coprecipitation, and physical adsorption of contaminants [11]. In the environment, biochar can alter the biogeochemistry of As because biochar can promote electron transfer between oxidants and reductants in soils and sediments [12]. However, over time or over redox cycles, biochar can undergo weathering and degradation, leading to a decrease in its structural integrity and stability [13,14]. These changes in its stability and structure can generate additional pores or loading sites capable of retaining As, which may increase the (i)mobilization of As by biochar. Weather biochar may also release or sorb DOC from solution, impacting microbial processes and possibly Eh. Despite the possibility of increasing As availability due to the application of organic C in the environment, biochar *in natura* or with chemical modification has been applied in aerobic and anaerobic environments as a strategy to immobilize As [15, 16]. However, little is known about the mobility and speciation of As, in particular organic species, caused by the application of biochar pyrolyzed at different temperatures to sediment under fluctuating redox conditions.

Our hypothesis is that increasing the pyrolysis temperature can buffer the biogeochemical redox processes occurring within the sediment, as well as provide a large surface area sorbent, and thus reduce As availability and methylation. In this study, we quantified the effect of pyrolysis temperature and biochar application on the release and transformation of As in sediment subjected to redox fluctuations. We used ultraviolet-visible spectroscopy (UV–vis) to assess the quality of DOC and oxidation state specific hydride generation-inductively coupled plasma mass spectrometry (ICP-MS) with cryotrapping to assess dissolved As speciation. In application, we combined X-ray photoelectron spectroscopy and time-of-flight secondary ion mass spectrometry to investigate the chemical state and spatial distribution of chemical elements in the sediment.

2. Materials and methods

2.1. Sediment sampling and characterization

The sediment was collected from the upper layer of soil (0–0.25 m) impacted by legacy contamination from a lead (Pb) and silver (Ag) ore refining plant in Apiaí , state of São Paulo, Brazil (24°30' S; 48°50' W). The site was used between 1940 and 1956 for smelting Ag and Pb ore, contaminating the surrounding soils through tailing disposal. The sampling site is located in the Atlantic Forest biome with recovering secondary vegetation, a sub-perennial tropical forest with a predominance of shrubs (*Leucaena* spp.) and grasses (*Pennisetum* spp.) [17].

The elemental content in the sediment was determined in triplicate by microwave-assisted acid digestion (Environmental Protection Agency – EPA - 3051 A method [18]) with the concentrations quantified by inductively coupled plasma mass spectrometry (Agilent 7900 ICP-MS; Agilent Technologies) equipped with an octupole collision/reaction. The As concentration was 18,675 mg kg^{-1}, a value higher than the intervention levels proposed by the Brazilian [19,20] and United States [21] Environmental Protection Agencies. The crystalline phases in the sediment and the tailings (source of contamination) were determined by Powder X-ray diffraction (XRD) [22] using a computer-controlled diffractometer (Smartlab, Rigaku) with Cu Kα radiation (0.1542 nm) - (40 kV and 40 mA) and a graphite monochromator. After obtaining the diffractograms, the positions of the peaks were corrected, and the crystalline phases were identified by the Match! Program (Crystal Impact, Bonn, DE). Details of the methodology and chemical composition of the sediment can be consulted in electronic annex (EA).

2.2. Production and characterization of the biochar

The biochar was produced from sugarcane straw (*Saccharum officinarum*) collected from a recently harvested agricultural area. Sugarcane straw was chosen as a feedstock due to its potential use in the production of bioenergy in Brazil [23]. After collection, the straw was air-dried before being placed in a double-sealed reactor (reactor with no oxygen). The reactor was heated at a rate of 5 °C min^{-1} and the final pyrolysis temperatures of 350 (BC350), 550 (BC550), and 750 (BC750) °C were maintained for 1 h. The pyrolysis temperatures were selected based on the physicochemical changes that each temperature can provide to the biochar and thus promote electrochemical changes in the sediment solution that can affect the geochemistry of As.

The composition and morphology of biochar and sugarcane straw was determined. The elemental composition of the biochar and sugarcane straw was ascertained according to the EPA - 3051 A method [18] (EA - Table A.1). Carbon and N contents of the biochar were determined by an elemental analyzer (LECO CN928 Series Macro). The contents of ash and fixed C were estimated by mass loss using the muffle method [24]. Dissolved organic carbon (DOC) was extracted according to the Analytical Methods Guide for Biochar [25]. The DOC content was quantified using an elemental TOC analyzer (TOC-L, Shimadzu). The morphology of the biochar was evaluated by scanning electron microscopy (FEI Quanta FEG-250) with a 15 kV beam and 250 × magnification, and the specific surface area of the biochar was estimated by N_2

sorption adjusted by the BET isotherm (Quantachrome NOVA 2200e) [26]. To investigate long range ordered phases in biochar produced by pyrolysis, synchrotron X-ray diffraction (S-XRD) was collected at 11-BM beamline of the Advanced Photon Source (APS) at the Argonne National Laboratory (Lemont, IL, USA).

2.3. Redox fluctuation experiment

To simulate the changes in redox conditions, a custom apparatus was constructed to control the level of water in contact with sediment (electronic annex - EA Fig. A.1). The apparatus had two orifices at the top to provide gas exchange between the external and internal environment, and entry and exit of water in the system simulated the movement of the water table to fill the vadose zone. The holes also served as a gateway for the platinum and Ag/AgCl electrodes used for monitoring pH and Eh during the experiment. The platinum wire electrode was fixed in the sediment core and remained fixed until the end of the experiment to avoid disturbances in the sediment immersed in water.

The Ag/AgCl electrode was periodically (every three days) placed in the solution present on the surface of the sediment so as not to come into contact with the sediment and was used to measure pH and as a reference electrode for Eh measurements. The Ag/AgCl electrode was calibrated with standard solutions of pH 4, 7, and 10 (ThermoFisher Scientific), and the platinum electrode was tested with 450 eV redox buffer solution and tap water as proposed by Fiedler et. al. [27]. The results of the platinum electrode test are shown in EA Table A.2.

The redox experiment was carried out with four replications using 100 g of sediment and 800 mL of ultrapure (1:8 w/v). The amount of biochar added to the sediment was 5% (w/w), a value widely reported in bibliographic references as sufficient for remediation of contaminated areas [28,29]. In addition to the biochar treatments, a control treatment (sediment without biochar) was conducted to monitor geochemical changes inherent to redox fluctuation.

The biochar samples were pre-incubated in the sediment for 30 d before starting the redox fluctuation experiment to allow adequate stabilization and initial aging of the biochar. The redox fluctuation was driven by two flooding cycles (reducing environment) and a draining cycle (oxidizing environment) accomplished by gravity drainage (without the use of pressure to remove water from the pores of the solid phase). The flooding cycles consisted of 30 d of inundation whereas the drainage cycle lasted for 10 d. The choice of flooding and drainage times were based on the time required for oxidation/reduction of As and Fe [30,31].

At the end of each flooding cycle, sediment and solution samples were collected inside an anaerobic chamber under N_2/H_2 (nominally 95/5%) gas mixture. The solution samples were filtered through a 0.22 μm nylon filter, stored in 5 mL cryovials (ThermoFisher Scientific) packed inside plastic bag with aneropacks (Mitsubishi gas chemical, Tokyo), and frozen at − 20 ºC until of analysis. Sediment samples were freeze-dried immediately for later analysis. The Fe content in solution was determined by Flame Atomic Absorption Spectroscopy – FAAS (iCE 3300 AA Spectrophotometer, ThermoFisher Scientific).

2.4. Content and aromaticity of dissolved organic carbon

The water samples were filtered (0.22 μm nylon filter) and stored in the dark in a refrigerator until analysis. The DOC content was quantified using an elemental TOC analyzer (TOC-L, Shimadzu), and the aromaticity of DOC ($SUVA_{254}$) was evaluated by using a Flame-S-UV–vis miniature UV–visible spectrophotometer equipped with a DH-mini UV–Vis–NIR Deuterium-Halogen Light Source (OceanOptics). The aromaticity of DOC (L mg^{-1} m^{-1}) was estimated by the relationship between the absorbance at a wavelength of 254 nm and the DOC content in the solution [32].

2.5. Spectroscopic analysis of sediment

X-ray photoelectron spectroscopy (XPS) analysis was performed on the freeze-dried sediment samples using an XPS/UVS spectrometer (SPECS System with PHOIBOS 150 Analyzer with Al/Ag double anode monochromator (10–14 kV energy) and with resolution < 1 eV. For all samples, the position of the binding energy peaks was calibrated by setting the C 1 s peak to 284.8 eV [33]. Baseline adjustment was performed using the Tougaard equation and the relative atomic content was calculated from the integration of the spectral lines of As 3d, Fe 2p, and C 1 s

The spectra were adjusted through Gaussian functions, and the As 3d spectra were analyzed taking into account the doublet due to spin-orbit division, with a BE difference of 0.7 ± 0.1 eV, equal FWHM and an area ratio between 3d 5/2 and 3d 3/2 3:2 contributions [34]. For Fe 2p, the core levels were in 2p 3/2 and 2p 1/2 doublets due to spin-orbit coupling. In addition, the positions of its satellites were defined and the possibility of having other multiplets in the spectrum was considered [35].

The spatial distribution as well as the location and relative abundance of chemical elements on the surface of the sediment was evaluated by the time-of-flight secondary ion mass spectrometry (ToF-SIMS; TOF SIMS V - ION TOF). The spectra and ToF-SIMS images were acquired in an area of 300×300 μm^2 (resolution of 256×256 pixels) using a pulsed Bi_3^{++} beam of 60 keV with an incidence of 45º. An electron flood gun (low energy electrons) was used to compensate for the process of surface charge accumulation during the analysis. The mass spectra of positive secondary ions were acquired for $m/z = 0$–1000 [36]. The detected intensities for secondary ion signals were warm color-coded according to the scale to obtain two-dimensional images (surface chemical maps). Beyond As, the elements C, Ca, and Fe were chosen because of the spatial correlation as representative of the main reactive components of the sediment.

2.6. Speciation of As in the sediment solution

The As species in solution were determined using an Agilent 7900 ICP-MS system (Agilent Technologies) coupled to customized HG and CT units [37,38]. Briefly, a sample is treated with sodium borohydride buffered with tris-hydrochloride at pH 6. The arsenicals are converted to volatile arsines and collected on a liquid nitrogen (LN_2) cryotrap. When the LN_2 is removed and the cryotrap heated the arsines are released to the ICP-MS in order of their boiling points (b.p.): arsine (AsH_3; b.p. = −62.5 °C), methylarsine (CH_3AsH_2; b.p. = 2 °C) and dimethylarsine [$(CH_3)_2AsH$, b.p. = 36 °C].

Only trivalent arsenicals are converted to arsines. Two aliquots of each sample are required to measure both As(III) and As(V). One sample is treated with L-cysteine hydrochloride monohydrate reducing agent (biochemical grade, Sigma-Aldrich) to a final concentration of 2% (w/v) and incubated at room temperature for 1 h before analysis [39]. This determines the total concentration of inorganic As, MMA(III+V), and DMA(III+V). Trivalent As species are determined from a 2nd sample run without the addition of the cystine reducing agent. The concentration of As(V) species is the difference between the total As and As(III) species.

As a quality control, in addition to the analytical blank, certified samples of drinking water (SRM 1643 f) and human urine (SRM 2669) from the National Institute of Standards and Technology (NIST) were analyzed. The drinking water standard was used to calculate the percentage of total As recovery obtained by summing the species and comparing to the total As obtained by the single measurement in ICP-MS. Standard Reference Material (SRM) 2669 Arsenic Species in Frozen Human Urine (NIST, US Department of Commerce) was used for quality control of the As speciation analysis by HG-CT-ICP-MS.

All sediment solution samples had total As levels determined by ICP-MS. The percentage of recovery of the total As from the drinking water standard was 92%. Similar recoveries were reached for As species

measured by HG-CT-ICP-MS in human urine: 90% (inorganic AsIII+V), 84% (MMAIII+V), 88% (DMAIII+V), and 93% (Total As, i.e., sum of As species). The sediment solution samples had an average percentage of total As recovery of 85.2%.

2.7. Statistical analysis

The data were submitted to the Shapiro-Wilk normality test ($p < 0.05$). Due to the non-normality of the data, the data were compared by the Bootstrap test ($p < 0.05$), which compares the mean through the confidence interval generated by 1000 random resampling with replacement [40].

The results of the geochemical changes of the sediment solution caused by the redox fluctuations were initially submitted to the Levene homoscedasticity test ($p < 0.05$). Subsequently, the differences in the content of the elements along the redox cycles were tested by the generalized linear mixed model (GLMM) using the software program R 2020 (R Core Team, Vienna, Austria). Pyrolysis temperatures were considered fixed effects while repetitions and redox cycles were considered random effects. The treatments were classified by the Bootstrap post hoc test ($p < 0.05$).

The autocorrelation and spatial correlation of chemical elements measured by TOF-SIMS were evaluated by the global and bivariate Moran indices. For this, the intensity data were converted into "raster" files and later analyzed in the R software (R Core Team, Vienna, Austria). The Global Moran index can comprehensively detect the spatial auto-phase size of spatial elements in a given area and is generally used to study the spatial pattern of geographic features and their time evolution analysis [41].

The bivariate Moran index was applied to evaluate the spatial relationship between the chemical elements of the sediment. This analysis provides an idea of the intensity and the locations when having significant correlation, and also indicates the presence of clusters with high values of the element close to high values of covariates (high-high); high of the element next to low values of covariates (high-low); low of the element close to high values of covariates (low-high); and low of the element close to low values of covariates (low-low) [42].

3. Results and discussion

3.1. Biochar structure

The pyrolysis temperature strongly influenced the chemical and structural composition of the biochar (EA Fig. A.2). In general, increasing the pyrolysis temperature concentrated C and ash in the biochar structure and reduced the DOC content. During biochar production, the loss C results in depolymerization and volatilization thermally sensitivite C [43,44]. Structural reorganization during pyrolysis is known [45] to generate a graphene like structure with surficial pores (EA Fig. A.3), resulting in a concomitant increase in the specific surface area of the biochar (EA Fig. A.2F).

The pyrolysis temperature also altered the long-range ordered phases present in the biochar, as determined by S-XRD (Fig. 1). The diffractogram of BC750 biochar had more and sharper peaks than that of BC550 biochar. It is also worth noting that the BC350 sample did not have peaks in the diffractogram above the background. This trend is consistent with an increase in the number and ordering of phases with increasing pyrolysis temperature.

The S-XRD analysis also identified specific phases within the biochar. Peaks in diffractograms of BC550 and BC750 indicate the presence of SiO_2, $CaCO_3$, graphite, and graphene, consistent with prior observation [46,47]. The peaks also indicate the presence of other carbonate and phosphate phases, such as Na_2CO_3 and $Ca_5(PO_4)_3$ [25]. The increase in ordered phases associated with carbonate and phosphate in BC550 and BC750 is consistent with these temperatures favoring the increase of ash contents in biochar (EA Fig. A.2C). In general, the presence of carbonate and phosphate can affect the dynamics of As [48], either by changing the pH, buffering the Eh, or by competition between arsenate and phosphate for sorption sites on mineral surfaces. Particularly for the BC750 diffractogram, there are peaks that could not be assigned, suggesting that additional phases may be present.

3.2. Redox changes in solution

Throughout the time course of the experiment, the redox and pH generally followed similar trends in unamended and biochar amended sediments. The initial Eh of ~350 mV decreased to < 0 mV of the course

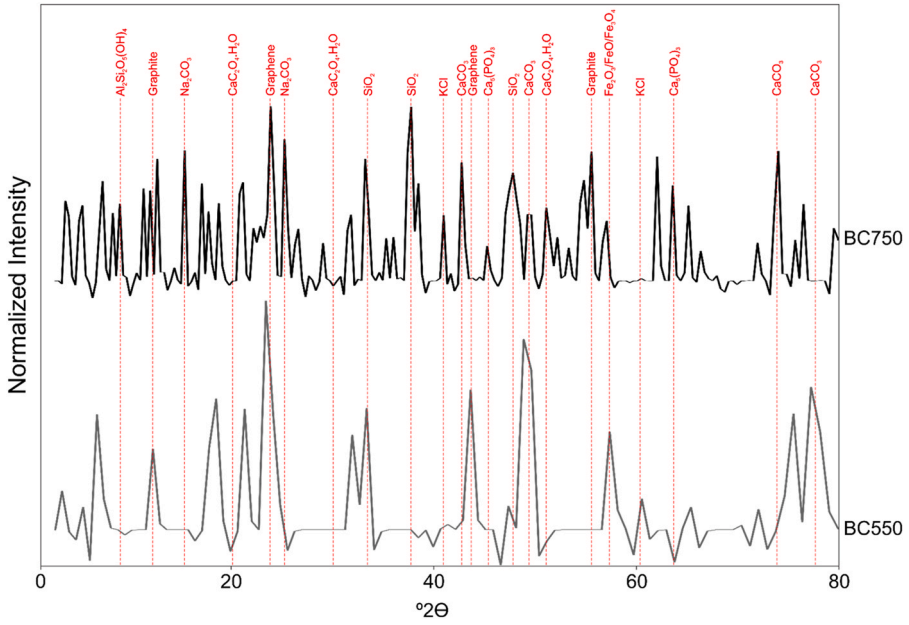

Fig. 1. Synchrotron X-ray diffraction patterns (λ = 0.459 Å) of pyrolyzed biochar samples at 550 (BC550) and 750 °C (BC750). Vertical dashed red lines represent the main diffraction peaks of the biochars.

of the first 30-day flooding; this change was accompanied by an increase in pH from ~6.6 to ~7.0 for all trials. During the 10-day drainage cycle, the Eh increased to ~100 mV before decreasing in the second 30-day flooding to Eh < 0 mV.

In general, biochar application resulted in greater pH and Eh values across the experiment (Fig. 2). The buffering of the redox potential by biochar may result from added redox active functional groups [49,50] as well as aromatic C [51]. The biochar has different functional groups with a range of electronegativities present on its surface, and this makes the biochar capable of either donating electrons or accepting electrons [52,53], thus regulating the redox potential of the environment. In addition, the exogenous supply of C in the environment modulates the microbial community by accelerating or reducing the activity of microorganisms responsible for C degradation [54].

3.3. Dissolved organic carbon

For all experimental conditions, the DOC release increased during the course of the redox fluctuation experiment (Fig. 3). The decomposition of organic C under partial or total anoxic conditions yields an enrichment of water-soluble intermediate metabolites [55] as a result of restricted and incomplete degradation. Consequently, DOC increases strongly during flooding [56] cycles. For the sediment and all biochar-amended sediments, the DOC released during the second flooding cycle exceeded that released during the first by approximately three-fold (Fig. 3).

The aromaticity of DOC (Fig. 3B and D) was affected by successive redox fluctuations, with aromaticity decreasing in the second flooding cycle. For both flooding cycles, the DOC in solution decreases but the DOC aromaticity (as judged by SUV_{254}) increases with increasing pyrolysis temperature. It is worth noting that there was less water extractable DOC in high temperature biochar (Fig. A.2E). High temperature pyrolysis also produced biochar with a greater specific surface area (Fig. A.2F), suggesting it may have a higher sorption capacity for DOC [57].

3.4. Arsenic in the solution

Similar to DOC, the total As content in solution increased on average five-fold in the second flooding cycle compared to the first (Fig. 4) for both the unamended and biochar-amended sediment. The oxidation and reduction processes from one cycle to another can destabilize the structure of As and Fe minerals of low crystallinity as well as increase the activity of microorganisms to the point of favoring biotic reductive dissolution [58,59]. For As(III) in particular (Fig. 5), a dramatic increase concentration (from < 10–2000–4000 mg L^{-1}) was observed from the 1st to 2nd redox fluctuation. As(V) contents increased as well, but was a much small effect for all but the sediment with no biochar application [58].

Biochar application had contrasting effects during successive flooding cycles. In the first flooding cycle, there was no effect of biochar application in the sediments. Interestingly, the control of the second

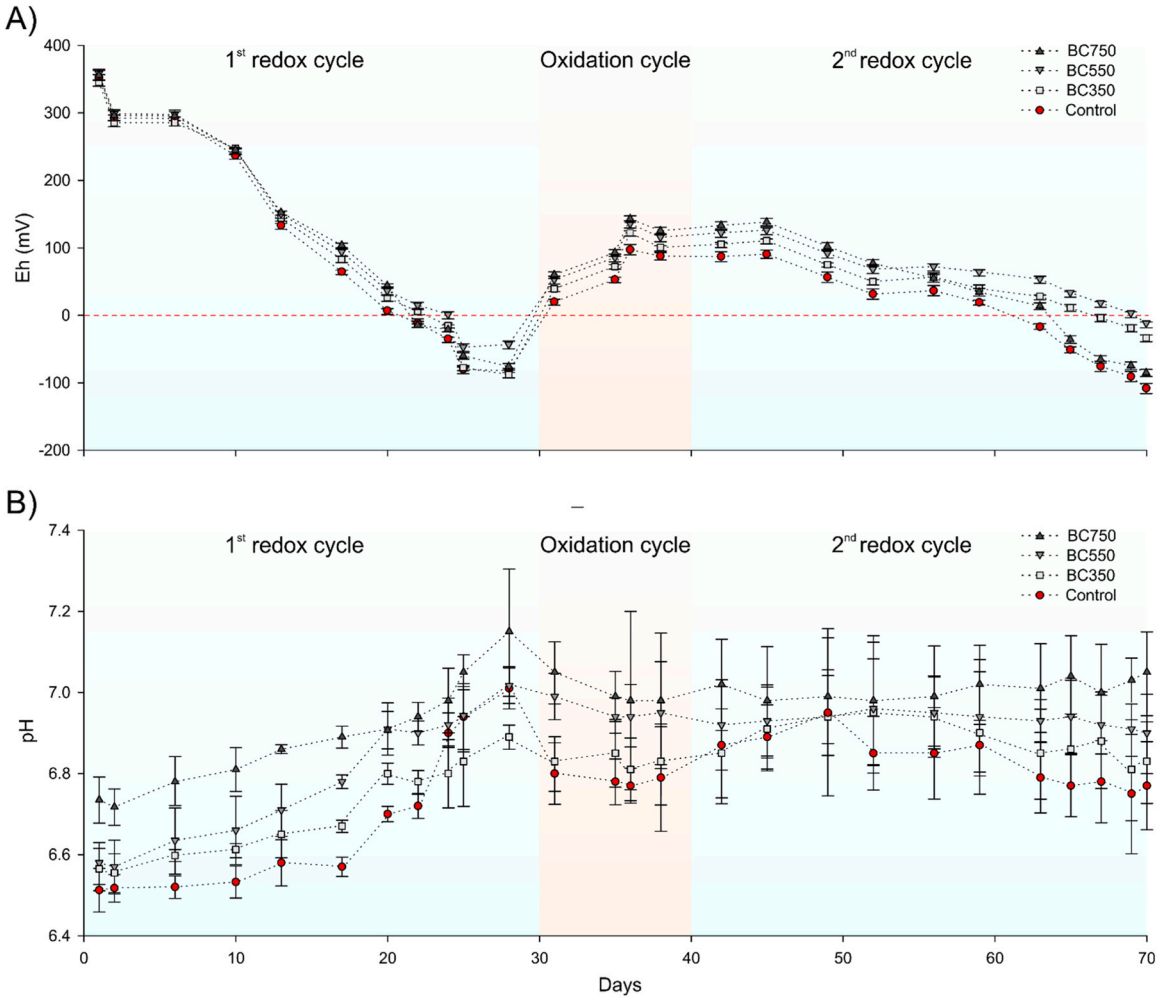

Fig. 2. Variation of redox potential - Eh (A) and pH (B) in a sediment amended with biochars subjected to redox fluctuation. BC350, BC550, and BC750 are biochars pyrolyzed at 350, 550, and 750°C, respectively. Bars represent the standard deviation of the samples (n = 4).

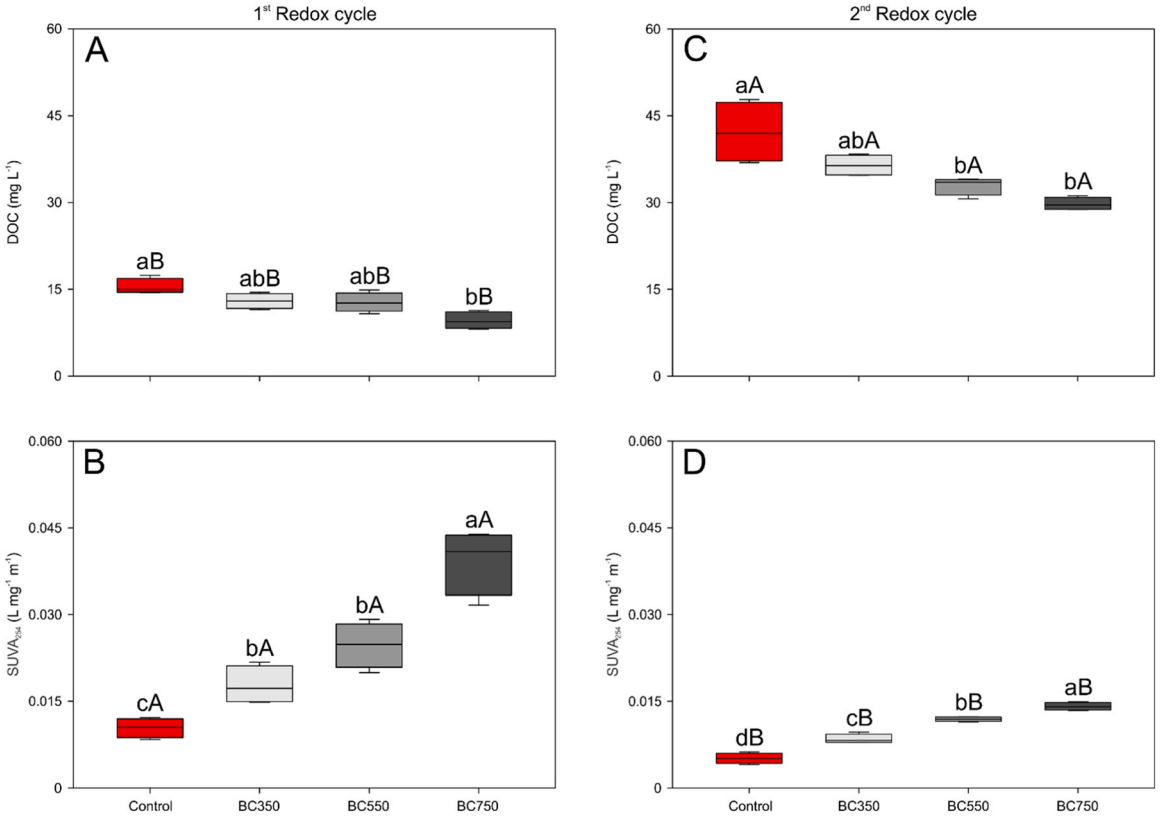

Fig. 3. Dissolved organic carbon (DOC) contents (A, C) and aromaticity of DOC ($SUVA_{254}$) (B, D) in the solution of a sediment amended with biochars subjected to redox fluctuation. BC350, BC550, and BC750 are biochars pyrolyzed at 350, 550, and 750 °C, respectively. Lowercase letters compare treatments, while uppercase letters compare sediment wetting cycles (Bootstrap test, $p < 0.05$). Bars represent the standard deviation of the samples (n = 4).

redox cycle had a dissolved As concentration ~ seven-fold higher that the control during the first flooding event. However, biochar applications were more efficient in decreasing As solubility in the second flooding cycle, with an average of ~1900 mg L^{-1} lower As concentration than the control (Fig. 4A). Specifically, the application of biochar reduced the As(V) content by 2100 mg L^{-1} compared to the control; low-temperature biochars (BC 350 and BC 550) also reduced the formation of As(III) species in solution in the second flooding cycle (Fig. 5). It is worth noting that the BC350 and BC550 amended sediments had greater Eh values during the second redox fluctuation (Fig. 2), consistent with decrease in dissolved As(III).

The application of biochar and the flooding cycle altered the Fe contents in solution (Fig. 4B and D). From the 1st to the 2nd flooding cycle, there was a five-fold increase in the Fe content in solution (from <120–120–240 mg L^{-1}), with a greater effect for the sediment without biochar amendment. Although biochar may be a source of Fe for the sediment, the application of biochar resulted in lower concentrations of Fe in solution, possibly due to the inhibition of Fe reduction caused by the quality of carbon compounds (Fig. 3B and D) and Eh buffering (Fig. 2).

The increase in the soluble Fe in solution during the second flooding cycle in sediment without biochar amendment is consistent with the larger concentration of As when compared to biochar amended sediments. Fe (oxyhydr)oxides have large sorption capacities for As (up to 1200 μM g^{-1} of As(V) and 800 μM g^{-1} of As(III) [60]) and their dissolution may result in the concomitant release of As. Thus, the inhibit of reductive Fe dissolution by biochar may result in increased retention of As by solid phases.

The difference in the effectiveness of biochar in immobilizing arsenic during flooding cycles may be due to the physicochemical properties of biochar caused by its reoxidation. Biochar has a high surface area and abundant pore spaces, which can adsorb As ions through physical and chemical interactions, and the retention intensity can be higher because of the structural changes in the biochar [61]. Additional groups such as hydroxyl (-OH), carboxyl (-COOH), and amine ($-NH_2$) can attract and bind As through electrostatic forces and surface complexation (EA Table A.5). In addition to functional groups, biochar produced at elevated temperatures can increase pH, possibly inducing arsenic to precipitate as less soluble, mobile, and bioavailable forms [62].

3.5. Organic species of arsenic

For all sediments and biochar-amended sediments, the organic As species MMA(III+V) and DMA(III+V) were detected, albeit at much lower concentrations than for inorganic species (Fig. 5). As with the inorganic arsenic species, the biochar application only affected the organic arsenic species concentrations in the 2nd flooding cycle (Fig. 5). Among the organic species, DMA was the As species least affected by the flooding cycles, with BC750 having the greatest (86% decrease) change in DMA(III+V) concentration. The results suggest that successive flooding cycles were critical for the release of inorganic As, with a lesser impact on organic As.

The application of biochar decreased the organic As concentrations (viz. DMA) in solution. The decrease may result from the sorption DMA (III+V) and MMA(III+V) to biochar. Linam et al. [63], however, did not observe sorption of DMA to biochar, which was attributed to DMA being a neutral and deprotonated molecule in which it interacts little with biochar. This suggests that biochars may not affect DMA sorption in soil. Another possibility is about the microbial formation of DMA may have been inhibited.

The As(V) reducing microorganisms use organic compounds as electron donors to reduce As(V) and obtain energy for their development [73]. The application of biochar may have inhibited by methylation by reducing the abundance altering the quality of DOC that couples to these

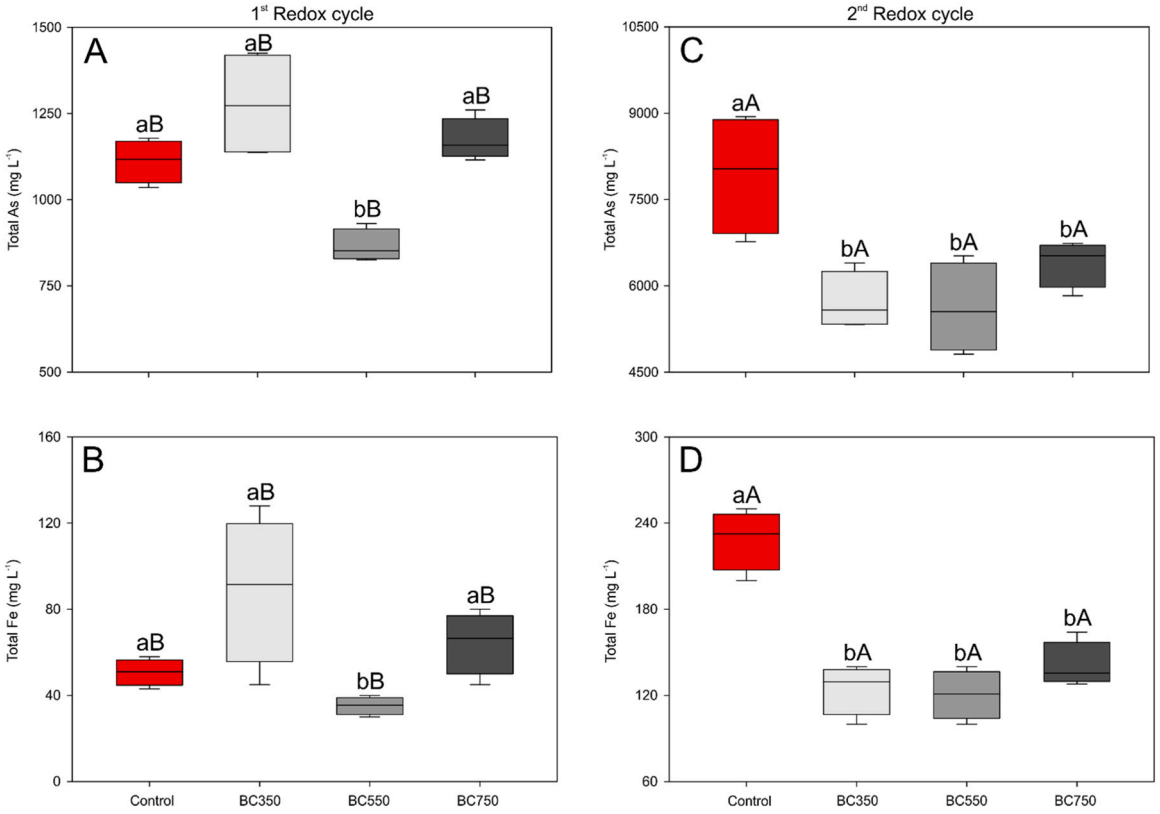

Fig. 4. Total contents of arsenic (A,C) and iron (B,D) in the solution of a sediment amended with biochars subjected to redox fluctuation. BC350, BC550, and BC750 are biochars pyrolyzed at 350, 550, and 750 °C, respectively. Lowercase letters compare treatments, while uppercase letters compare sediment wetting cycles (Bootstrap test, $p < 0.05$). Bars represent the standard deviation of the samples (n = 4).

reactions. Indeed, Yang et al. [64] noted that rice (*Oryza sativa*) straw biochar promoted an increase near the rhizosphere of As(V) and reduced microorganisms that harbor a gene associated with As reduction.

3.6. Spatial distribution and chemical state of elements in sediment

Geospatial analysis of TOF-SIMS images was used to identify changes in the distribution pattern of As, C, Fe, and Ca in the sediment (EA Table A.3). The global Moran index showed a reduction in the spatial autocorrelation of As from the first to the second flooding cycle, indicating that there may have been the dissolution and redistribution of concentrated As phases, such as those identified in the tailings (EA Fig. A.5). Islam et al. [65] evaluated the dissolution of As minerals in groundwater and verified a greater dissolution of As in arsenolite mineral through bio-weathering. We note that this is a component of the ore, and these processes may also result from dissolution of other concentrated As-bearing minerals found in the tailing (e.g., sinnerite ($Cu_6As_4S_9$), lammerite [$Cu_3(AsO_4)_2$]).

The dispersion of C on the map after the application of biochar was related to the pyrolysis temperature and flooding cycle (Fig. 6; EA Figs. A.6 and 7). There was a greater dispersion of C with biochar produced at higher pyrolysis temperatures, perhaps because of the lower number of functional groups present in the high-temperature biochars [44] may discourage organomineral interactions. Also, changes in the spatial distribution of C reflected changes in the quantity and quality of DOC, showing that there was a change in the C compartments as a function of the variation in the redox potential.

Moran's bivariate analysis showed that the spatial correlations of As with C, Fe, and Ca were influenced by the application of biochar and by the redox cycles (EA Figs. A.8, A.9, and A.10). In the first flooding cycle, the application of biochar reduced the spatial correlation of As with C, Fe, and Ca, whereas in the second flooding cycle, the correlation of As and C reduced in the control and increased in the treatments with biochar. It is possible that reoxidation of biochar surface group during the drying cycle may have resulted in increased negative charge, which may favor organometallic/mineral interactions. Furthermore, in the second redox cycle, there was a reduction of approximately 30% in the spatial correlation of As x Fe in the control (EA Fig. A.10). This result corroborates the previously reported discussion on the increase of As in the solution due to the reductive dissolution of Fe(III) minerals.

The differences in distributions of As, Fe and C in successive redox cycles is also reflected in the relative proportions of As, Fe and C species measured in the sediment by XPS (Fig. 7, EA Table A.4). Similarly to the sediment solution, the redox cycle and the biochar played an important role in the As, Fe and C species. At first, the application of biochar favored the availability of As(V) in solution due to the reduction of minerals containing Fe(III). The application of biochar resulted in a 20% increase in Fe(III) content when compared to the control, and part of this may be due to the release of DOC into the environment, which can promote microbial Fe reduction (EA Table A.5).

The second flooding cycle favored a greater proportion of As(III) and Fe(II) in the solid phase. This finding is in agreement with the results obtained in the sediment solution (Fig. 5), in which the fourfold increase in the content of As(III). These differences in the proportion of As(III) and Fe(II) as a function of the flooding cycle may be related to the stability of Fe(III) and As(V) minerals against the possibility of reductive dissolution. That is, in the first flooding cycle the reductive dissolution occurred to a lesser extent than in the second flooding cycle. We again note that mineralogical and microbiological processes may favor reduction in successive redox cycles [58,59].

The stability of soil Fe oxides under redox cycles may vary depending on several factors, such as the availability of electron acceptors and donors in the soil and/or sediment [66]. When subjected to redox fluctuations, Fe(III)-minerals can undergo transformations, leading to

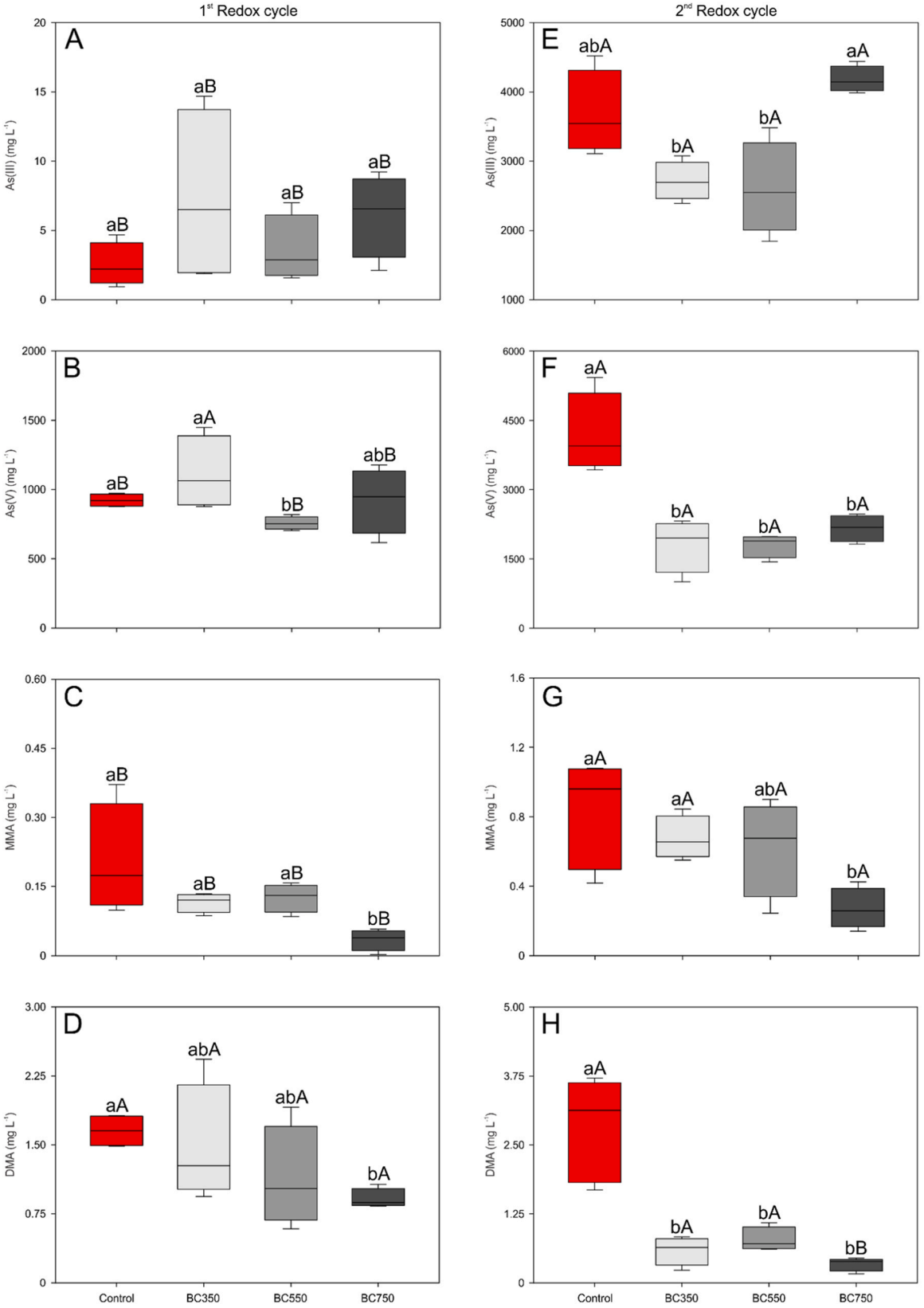

Fig. 5. Contents of arsenite [As(III)] (A, E), arsenate [As(V)] (B, F), Monomethyl [MMA(III+V)] (C, G), and Dimethyl arsenic [DMA(III+V)] (D, H) in the solution of a sediment amended with biochars subjected to redox fluctuation. BC350, BC550, and BC750 are biochars pyrolyzed at 350, 550, and 750 °C, respectively. Lowercase letters compare treatments, while uppercase letters compare sediment wetting cycles (Bootstrap test, $p < 0.05$). Bars represent the standard deviation of the samples (n = 4).

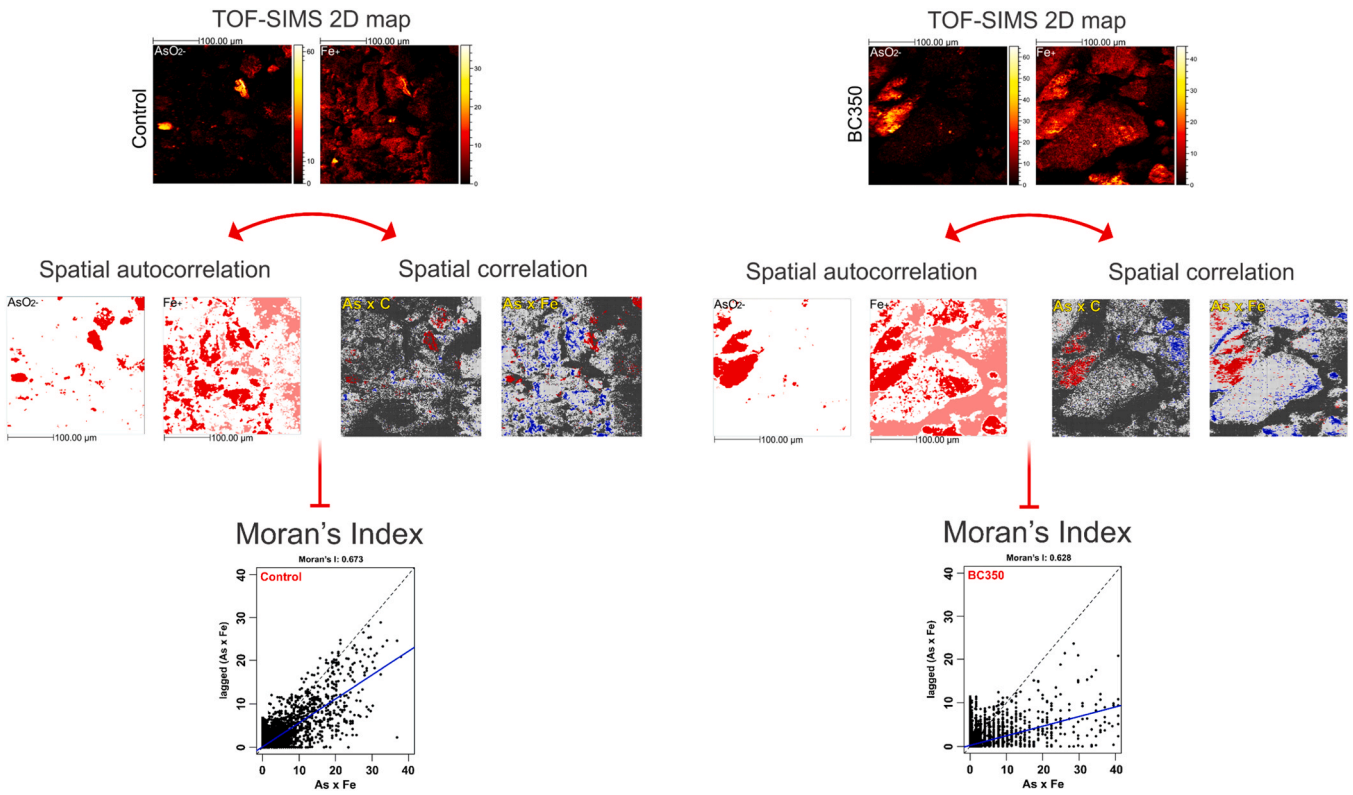

Fig. 6. 2D maps obtained from Time-of-Flight Secondary Ion Mass Spectrometry (TOF-SIMS) and analysis process of spatial distribution, autocorrelation, and spatial correlation of arsenic and iron in a sediment with and without biochar application. BC350 refers to a sediment amended with a biochar pyrolyzed at 350 °C. Details of the spatial distribution and correlation of chemical elements and other treatments can be found in the electronic annex.

alterations in their mineralogy and stability. Under anaerobic or low oxygen conditions, Fe(III)-minerals can be reduced by dissimilatory microbial reduction to Fe(II) forms. Conversely, during the oxidation or suboxic process, where the anoxic conditions are alleviated, the reduced Fe(II) can be re-oxidized back to Fe(III), resulting in secondary Fe(III) minerals. However, the reoxidation may not result in the original mineral structure, and the resulting Fe(III) forms may exhibit different physiochemical properties (e.g., ordering, particle size and morphology) compared to the original Fe(III) minerals, which in part depends on specific environmental conditions (e.g., pH and carbon content) [67]. It is worth mentioning the greater presence of carbon in solution after the first redox cycle, which may have played an important role in the regulating the stability of reprecipitated Fe(III) minerals from the first reduction cycle.

Among biochars, As availability may have been affected by solid-phase C quality. In the first flooding cycle, an organometallic complex was detected in the solid phase, and there were few functional groups associated with the carbonyl of amide/carboxylic (C═O), carboxylate (O-C-O), with most of the C was associated with aromatic and phenolic groups. However, after the first flooding cycle, organometallic complexes were absent, and the proportion of functional groups associated with the carbonyl of amide/carboxylic (C═O), carboxylate (O-C-O) increased. This result may indicate decomposition/oxidation of organic matter [68,69] of the sediment, which is consistent with the observed increase in DOC and the spatial dispersion of C in the sediment.

The organometallic complex identified by XPS in the first flooding cycle does not discriminate which metal was associated with C nor does it discriminate whether this complex was formed by C from the biochar or the sediment. However, the biochar promoted the formation of an organometallic complex during the first flooding cycle may have played an important role in the immobilization of As(V) because in the second flooding cycle, the formation of an organometallic complex was not identified and there was a four times increase in the release of As into the solution.

3.7. Recommendation for future studies on biochar

In recent years, different feedstock and pyrolysis temperatures have been used in the manufacture of biochar for remediation of As-contaminated environments in different countries (EA Table A.6). The effectiveness of the biochar is closely related to the environmental conditions and the pyrolysis characteristics of the biochar. In this study, it was evident that the effectiveness of the biochar depended not only on the pyrolysis temperature but also on the redox conditions of the sediment. In general, the biochar had a maximum removal potential of 121 mg kg^{-1} of As(V) and 56 mg kg^{-1} of As(III) (EA Table A.6). The effectiveness of biochar in removing As(V) and As(III) shown by the studies in Table A.6 does not take into variations account in redox potential, which may interfere with the removal capacity and consequently the cost of remediation. From an economic point of view, biochar can be an advantage in remediation. For example, in 2020, biochar produced from wood and used in wastewater treatment was cost-effective ($91–319/t) compared to activated carbon ($1500/t) and zeolite ($6000/t) [70]. However, there is a need for further studies under actual field conditions that take redox variations into account and thus be able to project the real effectiveness and cost of remediation with biochar.

4. Final remarks

Biochar application and pyrolysis temperature impacted the availability of and distribution of As species in sediment, the concentrations and quality of DOC, the methylation of As, and the redox conditions of the sediment and the spatial distribution and oxidation state of the elements. Because of the supply of extra C in the sediment, DOC-biochar interaction may be an important, although underestimated, mechanism in guiding the mobility and, subsequently, the bioavailability of contaminants in sediments amended with biochar, especially on the organic species of As.

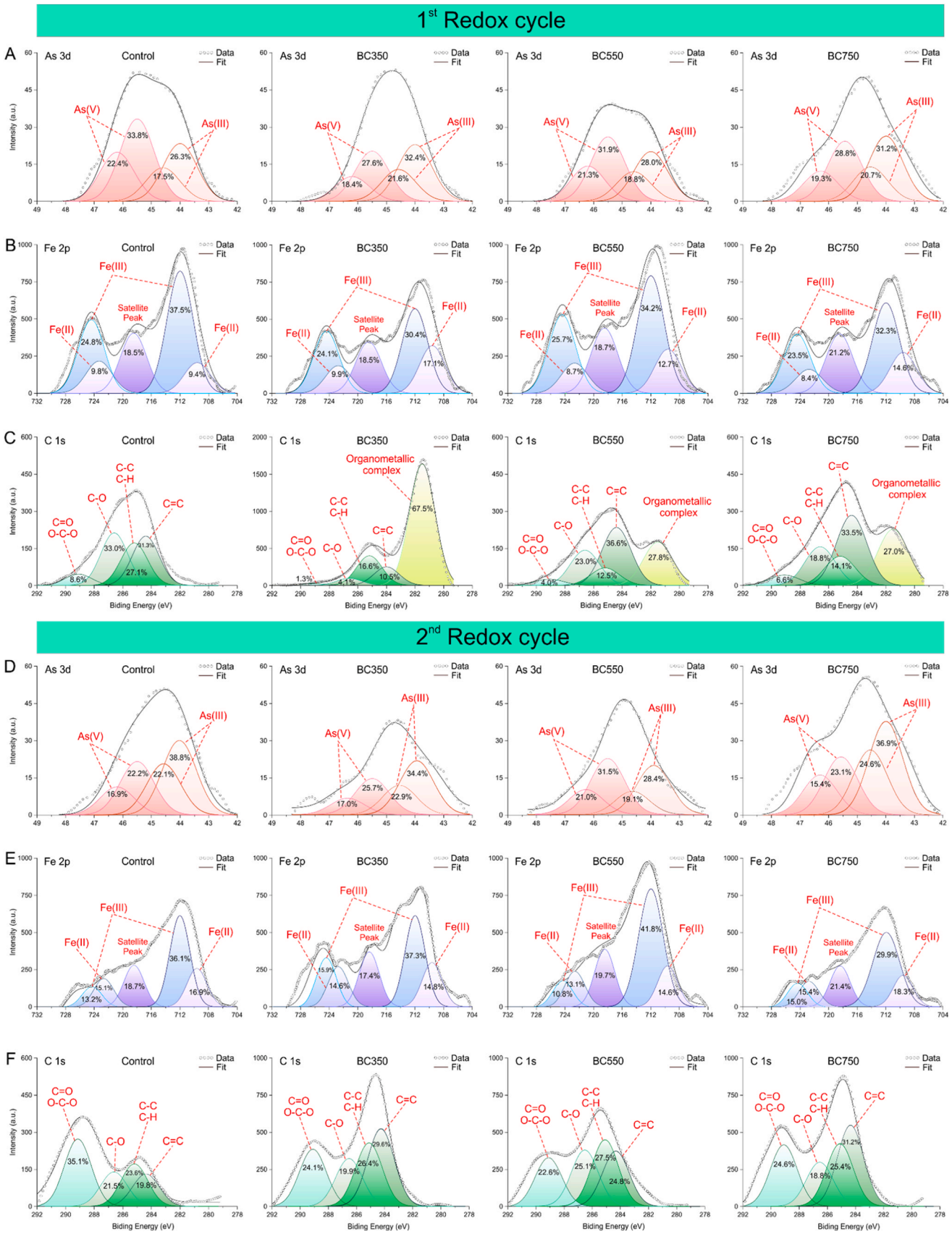

Fig. 7. X-ray photoelectron spectroscopy (XPS) analysis of arsenic 3d, iron 2p, and carbon 1 s from a sediment amended with biochars subjected to the first (A, B, C) and second (D, E, F) redox cycle. BC350, BC550, and BC750 are sediments amended with biochars pyrolyzed at 350, 550, and 750 ºC, respectively.

The impact of successive redox cycles in controlling biogeochemical processes that impact the mobilization of metals must be highlighted. The redox variations favored the dissolution of As minerals, increasing the As content in solution by seven times when subjected to redox variation. Furthermore, the redox cycle affected the reoxidation of functional groups present on the surface of the biochar altered the spatial distribution of C and favored the formation of organometallic/mineral complexes.

Based on our findings, in particular on MMA and DMA, we suggest that future studies be carried out to assess the potential fate and cycling of organic As species in naturally As-contaminated and biochar-altered environments. We also suggest the integrated use of advanced spectroscopic analysis (scanning X-ray transmission microscopy) and microbiological methods (gene sequencing) to provide deeper information on the organomineral/metallic interaction and the biogeochemical behavior of As in biochar-amended sediments under different redox conditions.

CRediT authorship contribution statement

The manuscript was written through the contributions of all authors. All authors have approved the final version of the manuscript.

Declaration of Competing Interest

The authors declare that they have no known competing financial interests or personal relationships that could have appeared to influence the work reported in this paper.

Data Availability

Data will be made available on request.

Acknowledgments

The 1st author gratefully thanks the São Paulo Research Foundation (FAPESP) (grants #2019/06897-9; 2020/13700-4) and the Brazilian Council for Scientific and Technological Development - Conselho Nacional de Desenvolvimento Científico e Tecnológico (CNPq) (grants #140830/2018-9) for the scholarships granted for this research. This study was partially funded by CNPq and the Coordination for the Improvement of Higher Education Personnel - Coordenação de Aperfeiçoamento de Pessoal de Nível Superior (CAPES) – Finance Code 001. This research was funded in part by the National Institute of Environmental Health Sciences (P42ES031007 and P30ES025128) and USDA National Institute of Food and Agriculture, Hatch project NC02713. We also thank Hannah Peel, Fred Stevie, Chuanzhen Zhou, Jenny Forrester, Wayne Robarge, and Renan Tavanti for their assistance. Part of this study was performed in part at the Environmental and Agricultural Testing Service laboratory (EATS), Department of Crop and Soil Sciences, at North Carolina State University and the Analytical Instrumentation Facility (AIF) at North Carolina State University, which is supported by the State of North Carolina and the National Science Foundation (ECCS-2025064). The AIF is a member of the North Carolina Research Triangle Nanotechnology Network (RTNN), a site in the National Nanotechnology Coordinated Infrastructure (NNCI). This research used resources of the Advanced Photon Source, a U.S. Department of Energy (DOE) Office of Science user facility operated for the DOE Office of Science by Argonne National Laboratory under Contract No. DE-AC02-06CH11357.

Appendix A. Supporting information

Supplementary data associated with this article can be found in the online version at doi:10.1016/j.jhazmat.2023.132308.

References

[1] FAO, UNEP, 2021. Global assessment of soil pollution - Summary for policy makers, Rome, 2021.
[2] Liu, S., Zhang, F., Chen, J., Sun, G., 2011. Arsenic removal from contaminated soil via biovolatilization by genetically engineered bacteria under laboratory conditions. J Environ Sci 23, 1544–1550. https://doi.org/10.1016/S1001-0742(10)60570-0.
[3] Podgorski, J., Berg, M., 2020. Global threat of arsenic in groundwater. Science (1979) 368, 845–850. https://doi.org/10.1126/SCIENCE.ABA1510/SUPPL_FILE/ABA1510_PODGORSKI_SM.PDF.
[4] Yang, X., Wen, E., Ge, C., El-Naggar, A., Yu, H., Wang, S., et al., 2022. Iron-modified phosphorus- and silicon-based biochars exhibited various influences on arsenic, cadmium and lead accumulation in rice and enzyme activities in a paddy soil. J Hazard Mater, 130203. https://doi.org/10.1016/J.JHAZMAT.2022.130203.
[5] Rinklebe, J., Kumpiene, J., du Laing, G., Ok, Y.S., 2017. Biogeochemistry of trace elements in the environment – Editorial to the special issue. J Environ Manag 186, 127–130. https://doi.org/10.1016/J.JENVMAN.2016.11.046.
[6] Yanan, Z., Li, H., Kai, Y., Yiqun, G., 2017. The role of dissolved organic matter in the competitive adsorption to goethite, during arsenic mobilization. Procedia Earth Planet Sci 17, 424–427. https://doi.org/10.1016/J.PROEPS.2016.12.107.
[7] Zhai, W., Guo, T., Yang, S., Gustave, W., Hashmi, M.Z., Tang, X., et al., 2021. Increase in arsenic methylation and volatilization during manure composting with biochar amendment in an aeration bioreactor. J Hazard Mater 411, 125123. https://doi.org/10.1016/J.JHAZMAT.2021.125123.
[8] Guerra, M.B.B., de Oliveira, C., Rocha de Carvalho, M., Silva, A.O., Santana Alvarenga, I.F., Barbosa, M.V., et al., 2023. Increased mobilization of geogenic arsenic by anthropogenic activities: The Brazilian experience in mining and agricultural areas. Curr Opin Environ Sci Health 33, 100472. https://doi.org/10.1016/J.COESH.2023.100472.
[9] de, D., Silva, C., Bellato, C.R., de, J., Marques Neto, O., Fontes, M.P.F., 2018. Trace elements in river water and sediments before and after a mining dam breach (Bento Rodrigues, Brazil). Quim Nova 41, 857–866. https://doi.org/10.21577/0100-4042.20170252.
[10] Quaresma, V.S., Bastos, A.C., Leite, M.D., Costa, A., Cagnin, R.C., Grilo, C.F., et al., 2020. The effects of a tailing dam failure on the sedimentation of the eastern Brazilian inner shelf. Cont Shelf Res 205, 104172. https://doi.org/10.1016/J.CSR.2020.104172.
[11] Lyu, H., Tang, J., Cui, M., Gao, B., Shen, B., 2020. Biochar/iron (BC/Fe) composites for soil and groundwater remediation: Synthesis, applications, and mechanisms. Chemosphere 246, 125609. https://doi.org/10.1016/J.CHEMOSPHERE.2019.125609.
[12] Amen, R., Bashir, H., Bibi, I., Shaheen, S.M., Niazi, N.K., Shahid, M., et al., 2020. A critical review on arsenic removal from water using biochar-based sorbents: The significance of modification and redox reactions. Chem Eng J 396, 125195. https://doi.org/10.1016/J.CEJ.2020.125195.
[13] Mukherjee, S., Sarkar, B., Aralappanavar, V.K., Mukhopadhyay, R., Basak, B.B., Srivastava, P., et al., 2022. Biochar-microorganism interactions for organic pollutant remediation: Challenges and perspectives. Environ Pollut 308, 119609. https://doi.org/10.1016/J.ENVPOL.2022.119609.
[14] Joseph, S., Husson, O., Graber, E.R., Van Zwieten, L., Taherymoosavi, S., Thomas, T., et al., 2015. The Electrochemical Properties of Biochars and How They Affect Soil Redox Properties and Processes. Agronomy 2015 5, 322–340. https://doi.org/10.3390/AGRONOMY5030322.
[15] Vithanage, M., Herath, I., Joseph, S., Bundschuh, J., Bolan, N., Ok, Y.S., et al., 2017. Interaction of arsenic with biochar in soil and water: a critical review. Carbon N Y 113, 219–230. https://doi.org/10.1016/j.carbon.2016.11.032.
[16] Premarathna, K.S.D., Rajapaksha, A.U., Sarkar, B., Kwon, E.E., Bhatnagar, A., Ok, Y.S., et al., 2019. Biochar-based engineered composites for sorptive decontamination of water: a review. Chem Eng J 372, 536–550. https://doi.org/10.1016/J.CEJ.2019.04.097.
[17] Santos, F.H. dos, Soares, M.B., Alleoni, L.R.F., 2022. Pristine and biochar-supported nano zero-valent iron to immobilize As, Zn and Pb in soil contaminated by smelting activities. J Environ Manag 321, 116017. https://doi.org/10.1016/J.JENVMAN.2022.116017.
[18] USEPA, 2007. Method 3051A: microwave assisted acid digestion of sediments, sludges, soils and oils. EPA, Washington.
[19] CETESB, 2016. Guide values for soil and groundwater in São Paulo, (2016). ⟨https://cetesb.sp.gov.br/aguas-subterraneas/valores-orientadores-para-solo-e-agua-subterranea/⟩ (accessed February 7, 2021).
[20] CONAMA, 2009. Resolution No. 420 on criteria and guide values for soil and groundwater quality, (2009) 20. ⟨https://cetesb.sp.gov.br/areas-contaminadas/wp-content/uploads/sites/17/2017/09/resolucao-conama-420–2009-gerenciamento-de-acs.pdf⟩ (accessed January 20, 2021).
[21] USEPA, 2020. Regional Screening Levels (RSLs) - Generic Tables, (2020). ⟨https://www.epa.gov/risk/regional-screening-levels-rsls-generic-tables⟩ (accessed August 3, 2020).
[22] Soukup, D.A., Drees, L.R., Lynn, W.C., 2008. Sampling soils for mineralogical analyses. In: Ulery, A.L., Drees, L.R. (Eds.), Methods of soil analysis Part 5—mineralogical methods. John Wiley & Sons, Ltd, pp. 1–11. https://doi.org/10.2136/sssabookser5.5.c1.
[23] Cherubin, M.R., Bordonal, R.O., Castioni, G.A., Guimarães, E.M., Lisboa, I.P., Moraes, L.A.A., et al., 2021. Soil health response to sugarcane straw removal in Brazil. Ind Crops Prod 163, 113315. https://doi.org/10.1016/J.INDCROP.2021.113315.

[24] ASTM, 2007. ASTM D1762–84 - Standard Test Method for Chemical Analysis of Wood, 2007. ⟨https://doi.org/10.1520/D1762–84R13⟩.
[25] Singh, B., Camps-Arbestain, M., Lehmann, J., 2017. Biochar: a guide to analytical methods. Taylor and, CSIRO, Boca Raton.
[26] Song, W., Guo, M., 2012. Quality variations of poultry litter biochar generated at different pyrolysis temperatures. J Anal Appl Pyrolysis 94, 138–145. https://doi.org/10.1016/J.JAAP.2011.11.018.
[27] Fiedler, S., Vepraskas, M.J., Richardson, J.L., 2007. Soil redox potential: importance, field measurements, and observations. Adv Agron 1–54. https://doi.org/10.1016/S0065-2113(06)94001-2.
[28] Tu, C., Wei, J., Guan, F., Liu, Y., Sun, Y., Luo, Y., 2020. Biochar and bacteria inoculated biochar enhanced Cd and Cu immobilization and enzymatic activity in a polluted soil. Environ Int. 137, 105576 https://doi.org/10.1016/J.ENVINT.2020.105576.
[29] El-Naggar, A., Shaheen, S.M., Hseu, Z.Y., Wang, S.L., Ok, Y.S., Rinklebe, J., 2019. Release dynamics of As, Co, and Mo in a biochar treated soil under pre-definite redox conditions. Sci Total Environ 657, 686–695. https://doi.org/10.1016/J.SCITOTENV.2018.12.026.
[30] Ginn, B., Meile, C., Wilmoth, J., Tang, Y., Thompson, A., 2017. Rapid iron reduction rates are stimulated by high-amplitude redox fluctuations in a tropical forest soil. Environ Sci Technol 51, 3250–3259. https://doi.org/10.1021/ACS.EST.6B05709/ASSET/IMAGES/LARGE/ES-2016-05709P_0004.JPEG.
[31] Kujala, K., Laamanen, T., Khan, U.A., Besold, J., Planer-Friedrich, B., 2022. Kinetics of arsenic and antimony reduction and oxidation in peatlands treating mining-affected waters: effects of microbes, temperature, and carbon substrate. Soil Biol Biochem 167, 108598. https://doi.org/10.1016/J.SOILBIO.2022.108598.
[32] Li, G., Khan, S., Ibrahim, M., Sun, T.R., Tang, J.F., Cotner, J.B., et al., 2018. Biochars induced modification of dissolved organic matter (DOM) in soil and its impact on mobility and bioaccumulation of arsenic and cadmium. J Hazard Mater 348, 100–108. https://doi.org/10.1016/J.JHAZMAT.2018.01.031.
[33] Martinson, C.A., Reddy, K.J., 2009. Adsorption of arsenic(III) and arsenic(V) by cupric oxide nanoparticles. J Colloid Interface Sci 336, 406–411. https://doi.org/10.1016/J.JCIS.2009.04.075.
[34] Viltres, H., Odio, O.F., Lartundo-Rojas, L., Reguera, E., 2020. Degradation study of arsenic oxides under XPS measurements. Appl Surf Sci 511, 145606. https://doi.org/10.1016/J.APSUSC.2020.145606.
[35] Gurgul, J., Łątka, K., Hnat, I., Rynkowski, J., Dzwigaj, S., 2013. Identification of iron species in FeSiBEA by DR UV–vis, XPS and Mössbauer spectroscopy: influence of Fe content. Microporous Mesoporous Mater 168, 1–6. https://doi.org/10.1016/J.MICROMESO.2012.09.015.
[36] Arenas-Lago, D., Andrade, M.L., Vega, F.A., Singh, B.R., 2016. TOF-SIMS and FE-SEM/EDS to verify the heavy metal fractionation in serpentinite quarry soils. Catena 136, 30–43. https://doi.org/10.1016/J.CATENA.2015.03.005.
[37] Matoušek, T., Wang, Z., Douillet, C., Musil, S., Stýblo, M., 2017. Direct speciation analysis of arsenic in whole blood and blood plasma at low exposure levels by hydride generation-cryotrapping-inductively coupled plasma mass spectrometry. Anal Chem 89, 9633–9637. https://doi.org/10.1021/ACS.ANALCHEM.7B01868.
[38] Matoušek, T., Currier, J.M., Trojánková, N., Saunders, R.J., Ishida, M.C., González-Horta, C., et al., 2013. Selective hydride generation-cryotrapping-ICP-MS for arsenic speciation analysis at picogram levels: analysis of river and sea water reference materials and human bladder epithelial cells. J Anal Spectrom 28, 1456–1465. https://doi.org/10.1039/C3JA50021G.
[39] Matoušek, T., Hernández-Zavala, A., Svoboda, M., Langrová, L., Adair, B.M., Drobná, Z., et al., 2008. Oxidation state specific generation of arsines from methylated arsenicals based on l-cysteine treatment in buffered media for speciation analysis by hydride generation-automated cryotrapping-gas chromatography-atomic absorption spectrometry with the multiatomizer. Spectrochim Acta Part B Spectrosc 63, 396–406. https://doi.org/10.1016/J.SAB.2007.11.037.
[40] Soares, M.B., Santos, F.H., Alleoni, L.R.F., 2022. Temporal changes in arsenic and lead pools in a contaminated sediment amended with biochar pyrolyzed at different temperatures. Chemosphere 287, 132102. https://doi.org/10.1016/J.CHEMOSPHERE.2021.132102.
[41] Zhang, X., Zhang, M., He, J., Wang, Q., Li, D., 2019. The spatial-temporal characteristics of cultivated land and its influential factors in the low hilly region: a case study of Lishan Town, Hubei Province, China. Sustainability 2019 11, 3810. https://doi.org/10.3390/SU11143810.
[42] Pusch, M., Oliveira, A.L.G., Fontenelli, J. v, Amaral, L.R.D., 2021. Soil properties mapping using proximal and remote sensing as covariate. Eng Agríc 41, 634–642. https://doi.org/10.1590/1809-4430-ENG.AGRIC.V41N6P634-642/2021.
[43] Al-Rumaihi, A., Shahbaz, M., Mckay, G., Mackey, H., Al-Ansari, T., 2022. A review of pyrolysis technologies and feedstock: a blending approach for plastic and biomass towards optimum biochar yield. Renew Sustain Energy Rev 167, 112715. https://doi.org/10.1016/J.RSER.2022.112715.
[44] Tomczyk, A., Sokołowska, Z., Boguta, P., 2020. Biochar physicochemical properties: pyrolysis temperature and feedstock kind effects. Rev Environ Sci Biotechnol 19, 191–215. https://doi.org/10.1007/s11157-020-09523-3.
[45] Chandra, S., Bhattacharya, J., 2019. Influence of temperature and duration of pyrolysis on the property heterogeneity of rice straw biochar and optimization of pyrolysis conditions for its application in soils. J Clean Prod 215, 1123–1139. https://doi.org/10.1016/J.JCLEPRO.2019.01.079.
[46] Maleki, A., Bozorg, A., 2023. Algal biochar of unique structure as a robust alternative to manipulate mixed-matrix membranes performance and fouling resistance. Results Eng 18, 101043. https://doi.org/10.1016/J.RINENG.2023.101043.
[47] Zhou, X., Moghaddam, T.B., Chen, M., Wu, S., Zhang, Y., Zhang, X., et al., 2021. Effects of pyrolysis parameters on physicochemical properties of biochar and bio-oil and application in asphalt. Sci Total Environ 780, 146448. https://doi.org/10.1016/J.SCITOTENV.2021.146448.
[48] Swaren, L., Safari, S., Konhauser, K.O., Alessi, D.S., 2022. Pyrolyzed biomass-derived nanoparticles: a review of surface chemistry, contaminant mobility, and future research avenues to fill the gaps. Biochar 2022 4, 1–17. https://doi.org/10.1007/S42773-022-00152-3.
[49] Goswami, L., Kushwaha, A., Singh, A., Saha, P., Choi, Y., Maharana, M., et al., 2022. Nano-biochar as a sustainable catalyst for anaerobic digestion: a synergetic closed-loop approach. Catalysts 12, 186. https://doi.org/10.3390/CATAL12020186.
[50] Deng, C., Lin, R., Kang, X., Wu, B., Wall, D.M., Murphy, J.D., 2021. What physicochemical properties of biochar facilitate interspecies electron transfer in anaerobic digestion: a case study of digestion of whiskey by-products. Fuel 306, 121736. https://doi.org/10.1016/J.FUEL.2021.121736.
[51] Carmona, M., Zamarro, M.T., Blázquez, B., Durante-Rodríguez, G., Juárez, J.F., Valderrama, J.A., et al., 2009. Anaerobic catabolism of aromatic compounds: a genetic and genomic view. Microbiol Mol Biol Rev 73, 71–133. https://doi.org/10.1128/MMBR.00021-08.
[52] S.O. Akpasi , I.M.S. Anekwe , J. Adedeji , S.L. Kiambi , S.O. Akpasi , I.M.S. Anekwe, et al. , 2022. Biochar Development as a Catalyst and Its Application, Biochar - Productive Technologies, Properties and Application [Working Title]. (2022). ⟨https://doi.org/10.5772/INTECHOPEN.105439⟩.
[53] Gasim, M.F., Choong, Z.Y., Koo, P.L., Low, S.C., Abdurahman, M.H., Ho, Y.C., et al., 2022. Application of biochar as functional material for remediation of organic pollutants in water: an overview. Catalysts 2022 12, 210. https://doi.org/10.3390/CATAL12020210.
[54] Wang, J., Xiong, Z., Kuzyakov, Y., 2016. Biochar stability in soil: meta-analysis of decomposition and priming effects. GCB Bioenergy 8, 512–523. https://doi.org/10.1111/gcbb.12266.
[55] Sahrawat, K.L., 2003. Organic matter accumulation in submerged soils. Adv Agron 81, 169–201. https://doi.org/10.1016/S0065-2113(03)81004-0.
[56] Hanke, A., Cerli, C., Muhr, J., Borken, W., Kalbitz, K., 2013. Redox control on carbon mineralization and dissolved organic matter along a chronosequence of paddy soils. Eur J Soil Sci 64, 476–487. https://doi.org/10.1111/EJSS.12042.
[57] Ambaye, T.G., Vaccari, M., van Hullebusch, E.D., Amrane, A., Rtimi, S., 2020. Mechanisms and adsorption capacities of biochar for the removal of organic and inorganic pollutants from industrial wastewater. Int J Environ Sci Technol 2020 18, 3273–3294. https://doi.org/10.1007/S13762-020-03060-W.
[58] Enright, A.M.L., Edwards, B.A., Ferris, F.G., 2019. Long range correlation in redox potential fluctuations signals energetic efficiency of bacterial Fe(II) oxidation. Sci Rep 2019 9, 1–8. https://doi.org/10.1038/s41598-019-40499-5.
[59] Pett-Ridge, J., Firestone, M.K., 2005. Redox fluctuation structures microbial communities in a wet tropical soil. Appl Environ Microbiol 71, 6998–7007. https://doi.org/10.1128/AEM.71.11.6998-7007.2005/ASSET/09BDB887-90AF-4541-8F47-918F348AC29E/ASSETS/GRAPHIC/ZAM0110560800004.JPEG.
[60] Dixit, S., Hering, J.G., 2003. Comparison of arsenic(V) and arsenic(III) sorption onto iron oxide minerals: Implications for arsenic mobility. Environ Sci Technol 37, 4182–4189. https://doi.org/10.1021/ES030309T/ASSET/IMAGES/LARGE/ES030309TF00006.JPEG.
[61] Sun, Y., Yu, F., Han, C., Houda, C., Hao, M., Wang, Q., 2022. Research progress on adsorption of arsenic from water by modified biochar and Its mechanism: a review. Water 14, 1691. https://doi.org/10.3390/W14111691.
[62] Zama, E.F., Li, G., Tang, Y.T., Reid, B.J., Ngwabie, N.M., Sun, G.X., 2022. The removal of arsenic from solution through biochar-enhanced precipitation of calcium-arsenic derivatives. Environ Pollut 292, 118241. https://doi.org/10.1016/J.ENVPOL.2021.118241.
[63] Linam, F., McCoach, K., Limmer, M.A., Seyfferth, A.L., 2021. Contrasting effects of rice husk pyrolysis temperature on silicon dissolution and retention of cadmium (Cd) and dimethylarsinic acid (DMA). Sci Total Environ 765. https://doi.org/10.1016/J.SCITOTENV.2020.144428.
[64] Yang, Y.P., Tang, X.J., Zhang, H.M., da Cheng, W., Duan, G.L., Zhu, Y.G., 2020. The characterization of arsenic biotransformation microbes in paddy soil after straw biochar and straw amendments. J Hazard Mater 391, 122200. https://doi.org/10.1016/J.JHAZMAT.2020.122200.
[65] Islam, A.B.M.R., Maity, J.P., Bundschuh, J., Chen, C.Y., Bhowmik, B.K., Tazaki, K., 2013. Arsenic mineral dissolution and possible mobilization in mineral–microbe–groundwater environment. J Hazard Mater 262, 989–996. https://doi.org/10.1016/J.JHAZMAT.2012.07.022.
[66] Rojas, C.A., de, A., Torio, S., Park, S., Bosak, T., Klepac-Ceraj, V., 2021. Organic electron donors and terminal electron acceptors structure anaerobic microbial communities and interactions in a permanently stratified sulfidic lake. Front Microbiol 12, 620424. https://doi.org/10.3389/FMICB.2021.620424/BIBTEX.
[67] Li, Q., Hu, W., Li, L., Li, Y., 2023. Interactions between organic matter and Fe oxides at soil micro-interfaces: Quantification, associations, and influencing factors. Sci Total Environ 855, 158710. https://doi.org/10.1016/J.SCITOTENV.2022.158710.
[68] Popolan-Vaida, D.M., Eskola, A.J., Rotavera, B., Lockyear, J.F., Wang, Z., Sarathy, S.M., et al., 2022. Formation of organic acids and carbonyl compounds in

n-butane oxidation via γ-Ketohydroperoxide decomposition. Angew Chem Int Ed 61, e202209168. https://doi.org/10.1002/ANIE.202209168.

[69] Kitz, F., Gómez-Brandón, M., Eder, B., Etemadi, M., Spielmann, F.M., Hammerle, A., et al., 2019. Soil carbonyl sulfide exchange in relation to microbial community composition: insights from a managed grassland soil amendment experiment. Soil Biol Biochem 135, 28–37. https://doi.org/10.1016/J.SOILBIO.2019.04.005.

[70] Sun, Y., Wang, T., Bai, L., Han, C., Sun, X., 2022. Application of biochar-based materials for remediation of arsenic contaminated soil and water: preparation, modification, and mechanisms. J Environ Chem Eng 10, 108292. https://doi.org/10.1016/J.JECE.2022.108292.